# CALIBRATION FOR INCREASED ACCURACY OF THE RANGE IMAGING CAMERA SWISSRANGER™

T. Kahlmann [a], F. Remondino [b], H. Ingensand [a]

[a] Geodetic Metrology and Engineering Geodesy (geomETH) - (kahlmann, ingensand)@geod.baug.ethz.ch
http://www.geometh.ethz.ch
[b] Photogrammetry and Remote Sensing - fabio@geod.baug.ethz.ch
http://www.photogrammetry.ethz.ch
Institute of Geodesy and Photogrammetry, ETH Zurich, 8093 Zurich, Switzerland

**KEY WORDS:** Camera, Range Imaging, Measurement System, Flash Ladar, Calibration, Accuracy, LIDAR, Laser scanning

**ABSTRACT:**
Range imaging is a new suitable choice for measurement and modeling in many different applications. But due to the technology's relatively new appearance on the market with a few different realizations, the knowledge of its capabilities is very low. In most applications, like robotics and measurement systems, the accuracy wanted, lies at some millimeters. The raw data of range imaging cameras do not reach this level. Therefore, the calibration of the sensors output is needed. In this paper some of the parameters which influence the behavior and performance of the range imaging camera SwissRanger™ (provided by the Swiss Center for Electronics and Microtechnology - CSEM) are described. Because of the highly systematic structure and correlations between parameters and output data, a parameter based calibration approach is presented. This includes a photogrammetric camera calibration and a distance system calibration with respect to the reflectivity and the distance itself.

## 1. INTRODUCTION

Range Imaging (RIM) is a fusion of two different technologies. According to the terminology, it integrates distance measurement as well as imaging aspects. It is a brand new measurement technique, not yet well known and investigated. Therefore both parts are shortly described in the following.

### 1.1 Electro-Optical Distance Measurement

The distance measurement principle of range imaging cameras is dominated by the time-of-flight principle. The time the light needs to travel from one point to another is directly proportional to the distance the light has traveled:

$$d = \frac{t}{2} \cdot c \tag{1}$$

where $d$ = distance between sensor and object
$c$ = speed of light
$t$ = time between emitting and receiving

Figure 1 points out two different distance measurement methods. A modulated radiation (e.g. light) is emitted, reflected by an object and partially mapped onto the receiver. Therefore, the distance sensor-object is half of the traveled distance of the radiation. Mainly, two different types of the time-of-flight principle are known:

1. Pulse Runtime Method
2. Phase Shift Determination

In the first case the runtime of a single pulse is directly measured. In order to reach a distance accuracy of a few millimeters, the clock accuracy has to be as low as a few picoseconds. Thus very good clock circuits are unavoidable. The EPF Lausanne (ETH Lausanne) has integrated such distance sensors in CMOS technology (Niclass et al., 2005). The sensor itself is an Avalanche Photo Diode (APD) with an external clock.

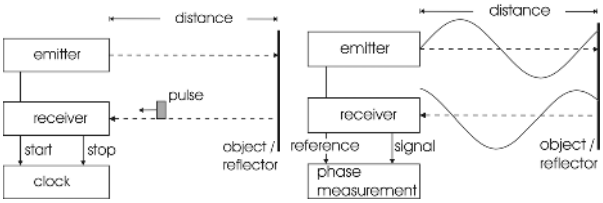


Figure 1. Time-of-flight distance measurement principle. Pulse Runtime (left) and Phase Shift (right).

On the other hand, the phase shift measurement principle avoids high precision clocks and uses more complex and integrative sensor design. The sensor investigated in this paper is based on this principle. The emitted (incoherent) light is modulated in amplitude with a sinusoidal modulation (Figure 2) whereas other methods are FMCW, pseudo-noise or polarization modulation. The reflected, sinusoidal modulated light is demodulated by means of four sampling points that are triggered to the emitted wave. Out of the four measurements c(τ0), c(τ1), c(τ2) and c(τ3) the phase shift $\varphi$, the offset B and the amplitude A can be calculated:

$$B = \frac{c(\tau 0) + c(\tau 1) + c(\tau 2) + c(\tau 3)}{4} \tag{2}$$

$$A = \frac{\sqrt{(c(\tau 0) - c(\tau 2))^2 + (c(\tau 1) - c(\tau 3))^2}}{2} \tag{3}$$

$$\varphi = \arctan\left(\frac{c(\tau 0) - c(\tau 2)}{c(\tau 1) - c(\tau 3)}\right) \tag{4}$$

The distance between the sensor and the object then can be calculated as follows:

$$d = \frac{\lambda_{\mathrm{mod}}}{2} \cdot \frac{\varphi}{2\pi} \qquad (5)$$

where $d$ = distance between sensor and object
$\lambda_{mod}$ = modulation wavelength
$\varphi$ = phase shift

As (Oggier et al., 2003) and (Seitz, 2005) have shown, the distance accuracy limitation, given by the nature of light for the investigated range imaging camera in this paper, is around 5 to 10 mm.

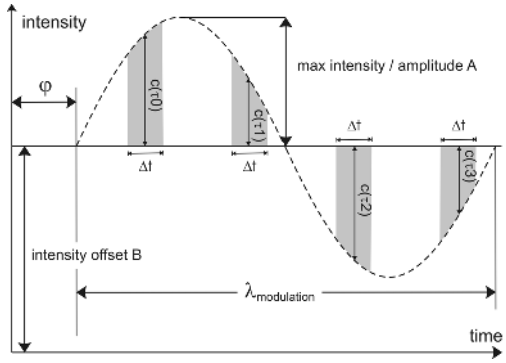


Figure 2. Phase shift distance measurement principle.

Because of the light's quantum structure the amplitude of light cannot be measured at a specific point of time. A time window Δt is necessary. Two opposed aspects define the size of the window. The quantum structure of the light is dominated by the light statistics at a higher Δt. But the higher Δt is, the lower the demodulation contrast is. According to (Lange, 2000) the sampling process is usually done with Δt at about half the modulation wavelength which results in a demodulation depth of about 64% (Figure 3).

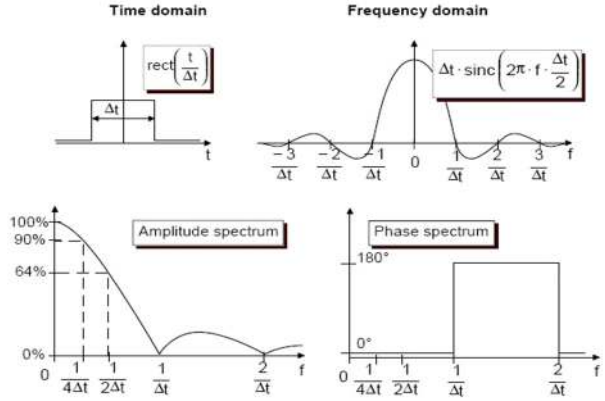


Figure 3. Sampling process and demodulation depth (Lange, 2000).

Irregularities in the sinusoidal continuous wave modulation with an uneven degree result in circular deviations of the linearity within the distance measurement (Lange, 2000). These deviations will be of importance in section 3.2.

### 1.2 Range Imaging Technology with CMOS sensor

The distance measurement principle outlined in section 1.1 is primarily able to measure distances in one direction at a time. Implemented in a scanning device (laser scanner, geodetic total station), a 3D capturing of the environment is possible. But the serial mode of operation still remains. Range imaging combines the distance measurement technology with the advantages of those of imaging arrays. Simplified, it just enables each pixel to measure the distance towards the corresponding object point. This is regarded as an array of range finders. Figure 4 presents the schematic principle of range imaging. A single signal emitter sends out modulated light. This light is reflected by an object partially back to the sensor and is mapped onto a custom-build solid state sensor by means of optics (not shown in the figure) and therefore onto the smart pixels which are able to measure the distance. The measured distances in connection with the geometrical camera relationships can be afterwards used to compute the 3D coordinates which represent a reconstruction of the imaged object.

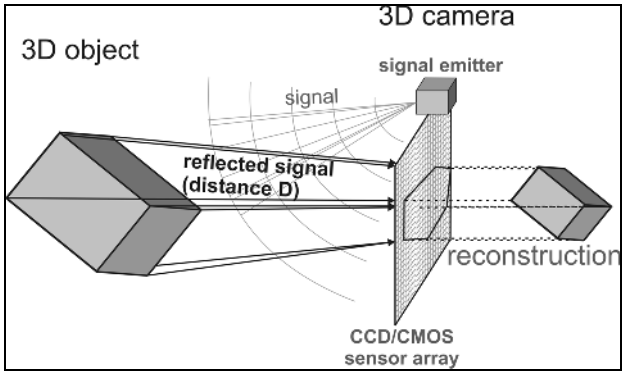


Figure 4. Range imaging principle.

One possible realization, similar but not equal to the one used in the investigated SwissRanger™ camera, is shown in Figure 5. By means of two photogates, the photon generated electrons are separated with respect to the modulation frequency. Two photogates allow only a one-tap or two-tap measurement, which means that only one resp. two of the four required intensities c(τi) are acquired. Therefore, this measurement has to be repeated four resp. two times.

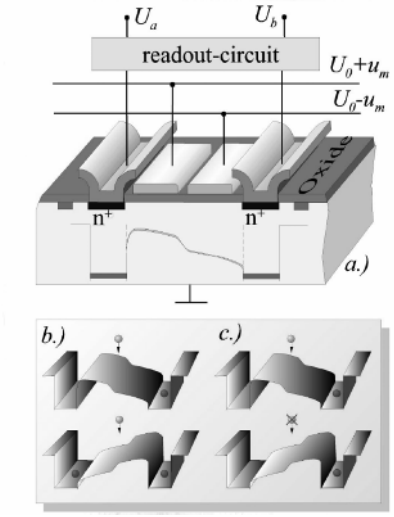


Figure 5. Lateral section of a RIM sensor from PMDTec (Möller et al., 2005).

The investigated SwissRanger™ SR-2 is shown in Figure 6. The emitting system consists of 48 LEDs. They are controlled simultaneously in order to reach a sufficient optical output power. The incoming radiation is mapped onto the sensor array, which is produced in a specialized mixed CCD and CMOS process.

Figure 6. SwissRanger™ SR-2.

Table 7 outlines some of the SwissRanger™'s characteristics. This sensor has a non-ambiguity distance of 7.5 m. Remarkable is the high number of pixels (nearly 20'000). The large pixel size corresponds to the high degree of integration of electronics.

| **SwissRanger™ SR-2** | | |
|---|---|---|
| **development** | *CSEM* | |
| **features** | | |
| number of pixel | 160 | 124 |
| pixel size | 39.2 µm | 54.8 µm |
| sensor field | 6.27 mm | 6.8 mm |
| mod. frequency | 20 MHz | |
| carrier wavelength | 870 nm | |
| non-ambiguity distance | 7.5 m | |
| Interface | USB 2.0 | |

Table 7. Characteristics of the investigated range imaging camera SwissRanger™ SR-2

The sensor can be run with different integration times. The integration time indicates how often/long the intensities c(τi) were collected and thus integrated. For a higher integration time, the electrons (also the photon generated ones) are collected for a higher number of cycles. The calculations are done afterwards.
Currently a new version of the sensor has been produced (SwissRanger SR-3000, http://www.swissranger.ch).

## 2. SYSTEM PROPERTIES

At the laboratories of the Institute of Geodesy and Photogrammetry (IGP), ETH Zurich, many different properties of the SwissRanger™ were investigated. The impact of the internal and external temperature influences on the distance measurements are reported in the next sections.

### 2.1 Influence of the Temperature onto the distance measurement

A problem very well known in semiconductor technology is the materials high respond to different temperatures and changes in the temperature. Especially in CCD and CMOS photo sensors an increased temperature causes a higher rate of thermal generated electrons. These electrons do not contain any usable information; they only fill the storage sites of the sensor equally and thus decrease and limit the usable optical capability for the actual signal to be derived. The saturation is reached sooner. In case of the SR-2, two different effects were observed.

#### 2.1.1 Internal Temperature

The first effect observed relates to an internal heating of the sensor. As seen in Figure 8, in the first minutes after the sensor starts working, the measured distance towards a fixed target increases. After a few minutes the process stabilizes. Therefore it is recommended to use the sensor in some kind of master mode, where it acquires continuously and stabilizes in temperature. But due to the fact that small gaps remain between the single frames, a cooling process takes place and small effects still remain as can be seen in Figures 8 and 9. The SR-2's concept does not provide an independent continuous mode. But nevertheless the effect remains regular and can therefore be factored in the calibration.

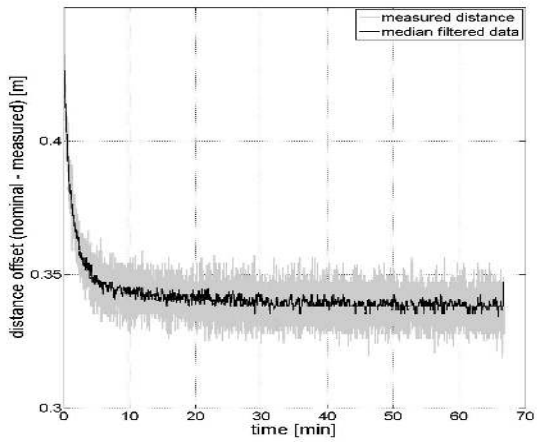


Figure 8: Distance offset drift (fixed target) caused by self-induced heating of the sensor.

#### 2.1.2 External Temperature

The second important influence of temperature on the distance measurement comes from the external temperature. To investigate this effect, the SwissRanger™ was placed in front of a fixed target. It has to be remarked that the sensor was not run in continuous mode, so far (separate thread in the mastering computer). Therefore, the trend of the single graphs in Figure 9 is valid for exactly the computer and program setup they were acquired with. But the main systematic behaviour can be seen. With a higher temperature the measured distance increases. It also can be pointed out that the effect is systematic and thus removable with a calibration procedure, as well. The determined drift lies around 8mm/°C.

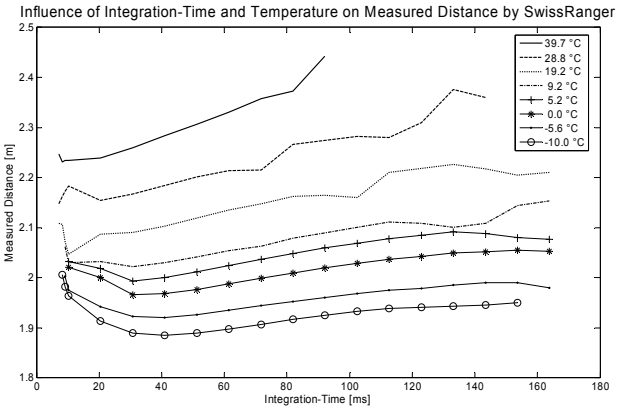


Figure 9: Relation between Integration-Time and Measured Distance with respect to different external temperatures

### 2.2 Distance Accuracy

Figure 10 shows the standard deviation for the distance measurements in every pixel. As it can be clearly seen, the

expected best accuracy of 5 to 10 mm was only achieved in the center of the sensor, where the illumination of the used object (white wall at approx. 2.453 m) was at its highest value (compare (Kahlmann, Ingensand, 2005)).

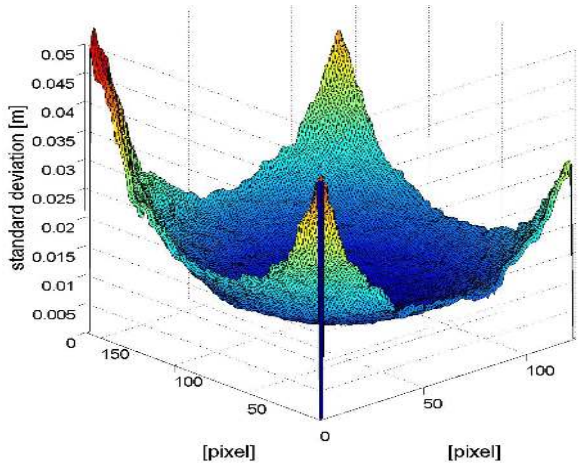


Figure 10: Standard deviation for a single distance measurement (of a white wall) measured and calculated for the whole sensor array. It was calculated out of 200 distance measurements in every pixel. The integration time was approx. 0.1 s.

## 3. SENSOR CALIBRATION

Due to the systematic effects, the sensor data shows that a calibration of the system is needed and possible. Different calibration approaches were followed up.

### 3.1 Photogrammetric Calibration

Accurate camera calibration and orientation procedures are necessary prerequisites for the extraction of precise and reliable 3D metric information from images. A camera is considered as calibrated if the focal lenght, principal point location and lens distortion parameters are known. In many applications, especially in computer vision, only the focal length is recovered while for precise photogrammetric measurements all the calibration parameters are generally employed. The choice of the camera model is often related to the final application and required accuracy. Projective or perspective camera model can be used but generally a precise sensor orientation is performed by means of a least squares bundle adjustment with additional parameters.

#### 3.1.1 Calibration procedure

For the TOF camera under investigation, different tests were performed. Due to the low resolution of the sensor, the selection of a suitable test field was crucial (Figure 11). A large test field would not allow the precise measurements of its targets due to the small sensor format. Large rounded targets occupy too many pixels. Squared targets have no well defined corners. Retro-reflective targets generated noise effects in the images. Moreover, the lightning of the room influences a lot the data acquisition. For all these reasons, a planar testfield whose targets are represented by NIR LEDs was build. These active targets can be automatically extracted from the intensity image provided by the camera due to their high intensity in the image. They are automatically extracted by means of a threshold and a centroid operator and used as input measures for the calibration procedure.

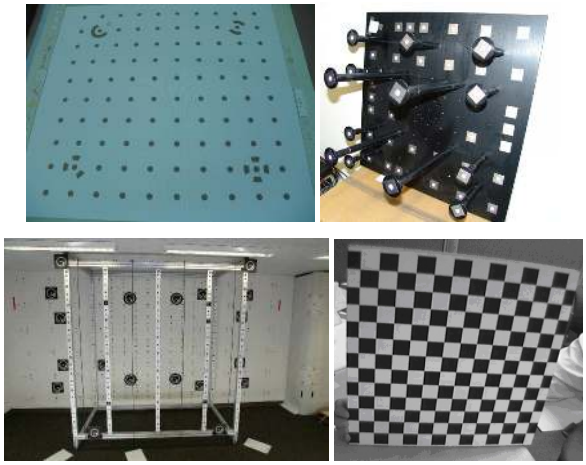

Figure 11: Different testfields used to calibrate the range imaging camera. None of them was usable for the calibration of the SR-2.

The calibration network of the TOF camera included 35 stations, well distributed, in particularly in depth direction as we used a planar testfield. After the self-calibrating bundle adjustment, the final standard deviations of the computed object points resulted $\sigma_x$ = 1.4 mm, $\sigma_y$ =1.3 mm, and $\sigma_z$ = 1.8 mm, which represent a relative accuracy of approximately 1: 270 in the testfield plane and 1:120 in the depth direction.
Between the additional parameters, only the first two terms of the radial distortions turned out to be statistically significant. The calibration network is shown in Figure 12.

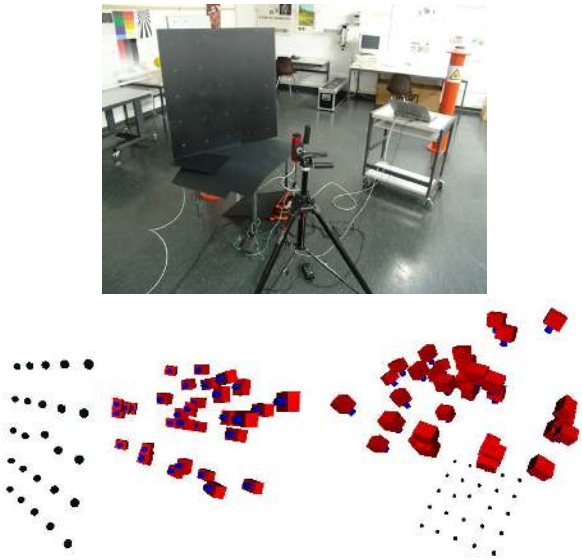

Figure 12: The final planar object with 25 infrared LED used to calibrate the TOF camera (above). The sensor connected via USB to a laptop is also visible in the foreground. The recovered camera poses during the calibration procedure (below).

### 3.2 Distance Calibration

The distance measurement accuracy of a single pixel in the center of the sensor has been investigated. In order to reach a high reliability of the acquired data, the calibration has been done on the high accuracy distance measurement track line available at the laboratories of the IGP. It is supported by an interferometer and the target carrier (trolley) runs fully automatically. The relative accuracy of the distance

measurement is around a few microns. The absolute accuracy of 0.1 mm is not reached due to the not standardized mounting of the SR-2. Therefore the absolute accuracy is about 1mm.

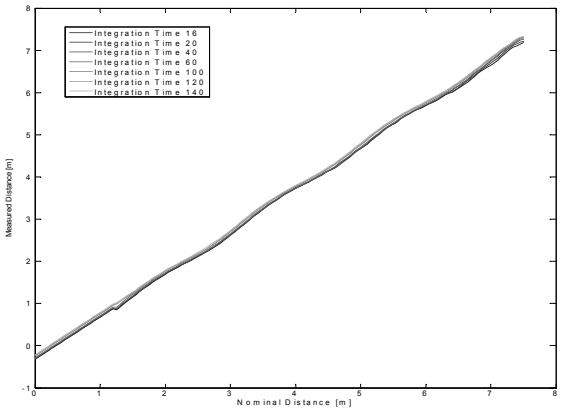


Figure 13: Filtered distance calibration data. The circular differences to the expected linearity can be clearly seen.

Two different parameters were varied for the calibration measurements. First all measurements were done with different integration times. Second, five targets with a different reflectivity were used (white, light grey, middle grey, dark grey and black).
The SR-2 has been placed along the track line. The targets were placed from 1.25 m to 7.5 m with steps of 0.05 m. At each position 10 distance measurement of one pixel (row:80, col:62) were made. These measurements were then median filtered. The trolley ran forth and back three times. The measurements were averaged to eliminate linear drift terms. At last the measurements were filtered over the distance range by means of an ideal low-pass-filter with a Hamming window.

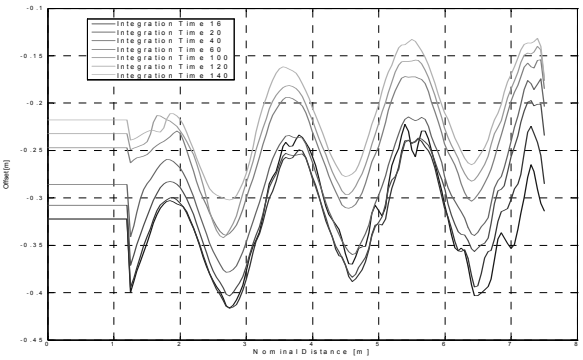


Figure 14: Final Look Up Table (LUT) data for different integration times. The reflectivity of the targets in comparison to the other influences is negligible.

Figure 13 shows the filtered data. The predicted circular effect can be clearly seen. Figure 14 shows the Look Up Table (LUT) data. This data is used for the correction of the distance data. Experiments with a modeling of the offset data with linear and cosine functions were done. But these did not brought better results. Therefore, a LUT is fully adequate.

### 3.3 Fixed Pattern Noise (FPN)

The distance calibration for a single pixel is not sufficient for the whole sensor array. Due to the high demand for time, a distance calibration cannot be done for all pixels. A simple strategy to reduce an offset is to acquire a Fixed Pattern Noise matrix. This matrix contains an individual offset for every pixel. To gain this matrix, an accurate procedure was developed. The SR-2 was mounted above a total station. The total station is able to measure coordinates of an object in front of the setup. In this case a white wall was chosen. By means of comparison between the nominal distances (calculated out of the nominal coordinates measured by the total station) and the data acquired by the camera, the FPN matrix can be determined.

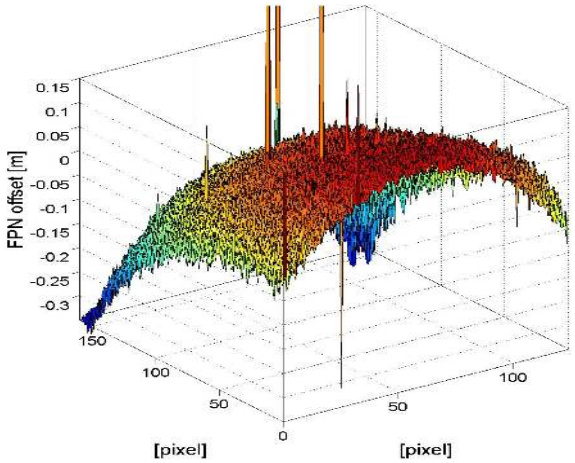


Figure 15: FPN matrix for the SR-2. Integration time was about 0.1 s, nominal distance 2.452 m. Damaged pixel can be depicted, too.

As Figure 15 depicts, the variation of the offset is not negligible and has to be considered in the calibration of the sensor. The range goes from about -0.3 m to about +0.15 m. A systematic tenor can be outlined. In this case this FPN matrix is only valid for an integration time of about 0.1 s. For every integration time, respectively every controlling computer/program setup such FPN is specific and has to be determined.

In Figure 16 and 17 the 3D comparisons between the data recorded before and after the calibration procedure are reported.

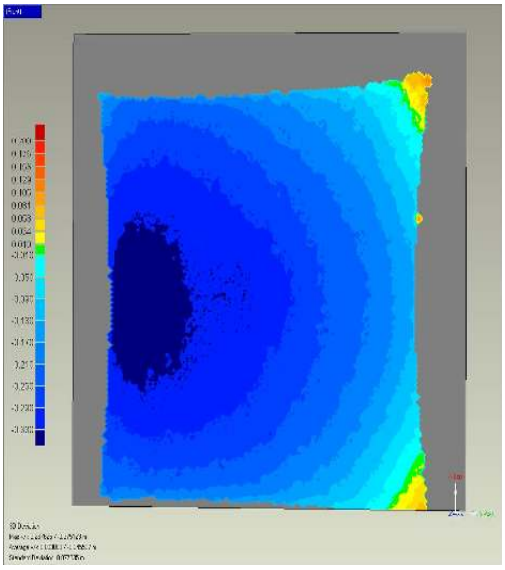

Figure 16: Deviations towards a flat wall before the calibration of the sensor. The highest deviation is around -30 cm (dark blue area).

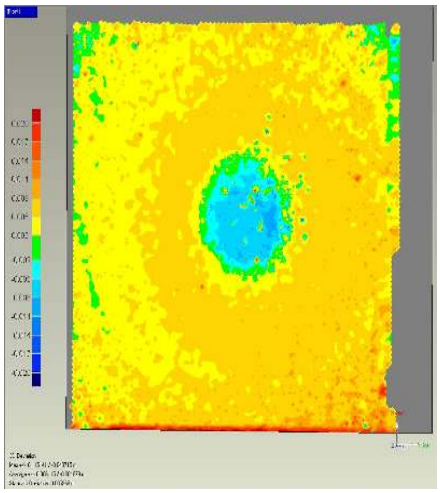

Figure 17: Deviations towards a flat wall after calibration of the sensor. The deviations are reduced from about -30 to +10 cm down to about ±1 cm after the calibration. Some systematic behaviour still remains.

## 4. APPLICATION AREAS OF RANGE IMAGING SENSORS

It is probable that RIM will replace close range scanners which work sequentially and cannot be used for kinematic approaches. Compared to existing scanner solutions, an additional advantage of RIM is the speed of the 3D data capture which is at the present technical state in the range of 20 Hz. This enables new application areas which are covered now by videogrammetry in the field of human or machine motion analysis. Additionally, range imaging sensors are very cheap in comparison to the existing technologies.

It is obvious that RIM can be advantageous for fast 3D face recognition, as stereoscopic image capture needs a wider field of view. Other applications can be envisaged in man-robot interaction environment to enable cooperative collaboration of man and machine. RIM will be used in the area of automotive sensors as so called precrash sensors to prevent the contact of pedestrians with the car engine or other solid parts. As a solution the hood will be lifted previously in order to damp the collision of person and car. Another potential application of the RIM is to control the airbag systems where RIM will determine the position of the passengers.

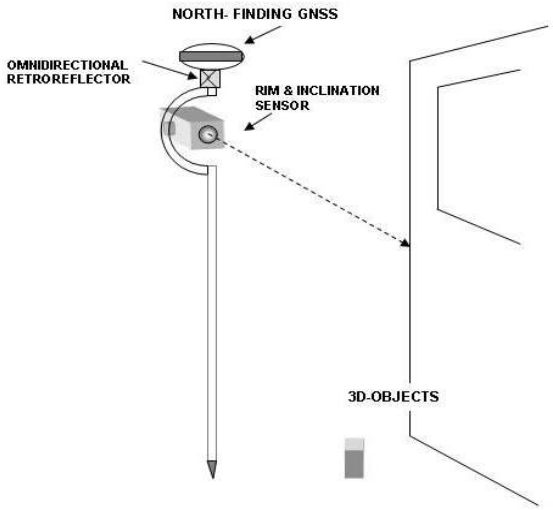


Figure 18: Geo-Probe application for RIM sensors.

In geodesy, RIM will promote the further integration of sensors into surveying instruments. After the integration of GPS and total station in Leica's Smart station, a combination of RIM, inclination sensor and north-finding GPS will enable new scenarios in data capture. As in most cases GPS can operate very closely to the object. The missing connection can be carried out by RIM technology. Analogous to the T-probe approach (Leica) in industrial metrology a so called Geo-Probe configuration allows for efficient data capturing if GPS generates additionally the orientation of the system (Figure 18; patent pending).

## 5. CONCLUSIONS

With the high-resolution range imaging camera SwissRanger™, a powerful new tool for many applications with a need for metrology is available. Many influencing parameters have an impact on the accuracy of the system. But due to their systematic appearance, they can be identified and removed within a calibration procedure.

In this paper, many different aspects of such a calibration were shown. It can be stated that a calibration is needed and possible. The achievable accuracy with respect to the calibrations depicted is around 1 cm. The recovered relative accuracy shows the potentiality of the TOF sensor for middle-accuracy applications, like autonomous navigation or real-time modeling. Further studies should be done in order to fully use the sensors abilities and exploit its potentialities.

## REFERENCES

CSEM - Centre Suisse d'Electronique et de Microtechnique SA: http://www.csem.ch

Kahlmann, T., Ingensand, H., 2005. Calibration and improvements of the high-resolution range-imaging camera SwissRanger™, *Proc. SPIE Vol. 5665*, pp. 144-155.

Lange, R., 2000. 3D Time-of-flight distance measurement with custom solid-state image sensors in CMOS/CCD-technology. *PhD-Thesis at the University of Siegen*, Siegen, Germany.

Möller, T., Kraft, H., Frey, J., Albrecht, M., Lange, R., 2005. Robust 3D Measurement with PMD Sensors. In: *Proceedings of the 1st Range Imaging Research Day at ETH Zurich*, Zurich, Switzerland, pp. "Supplement to the Proceedings".

Niclass, C., Besse, P.-A., Charbon, E., 2005. Arrays of Single Photon Avalanche Diodes in CMOS Technology: Picosecond Timing Resolution for Range Imaging. In: *Proceedings of the 1st Range Imaging Research Day at ETH Zurich*, Zurich, Switzerland, pp. "Supplement to the Proceedings".

Oggier, T., Lehmann, M., Kaufmann R., Schweizer, M., Richter, M., Metzler, P., Lang, G., Lustenberger, F., Blanc, N., 2003. An all-solid-state optical range camera for 3D-real-time imaging with sub-centimeter depth-resolution (SwissRanger), *Proc. SPIE Vol. 5249*, pp. 634-545.

Seitz, P., 2003. Unified analysis of the performance and physical limitations of optical range-imaging techniques. In: *Proceedings of the 1st Range Imaging Research Day at ETH Zurich*, Zurich, Switzerland, pp. 9-19.